Hindawi
Shock and Vibration
Volume 2021, Article ID 1082963, 21 pages
https://doi.org/10.1155/2021/1082963

Research Article

Development and Parametric Analysis of Vibration System Controlled by Hydraulic Shock Rotary Vibrator

Qichao Ren, Ziming Kou, Juan Wu, Tengyu Li, and Waled Yahya

National-local Joint Laboratory of Mining Fluid Control Engineering, School of Mechanical and Vehicle Engineering, Taiyuan University of Technology, No. 79 Yingze West Street, Taiyuan, Shanxi 030024, China

Correspondence should be addressed to Ziming Kou; zmkou@163.com

Received 30 August 2021; Revised 3 October 2021; Accepted 22 October 2021; Published 23 November 2021

Academic Editor: Roman Gabl

The improvement of the energy utilization rate of a hydraulic vibration-excitation system is critical to the research and development of hydraulic vibration equipment. In this paper, a hydraulic vibration-excitation system controlled by a new type of shock rotary vibrator is proposed. A system model considering the pipeline effect was established for the hydraulic shock phenomenon. In addition, the model was compared with the one that does not consider the pipeline effect. The effectiveness of the proposed model was verified experimentally. Finally, the shock phenomenon during the process of switching the working state of the vibrator and the influence of certain important parameters of the system on the vibration output were investigated based on the proposed model. The results showed that (1) the hydraulic shock phenomenon occurred when the working state of the hydraulic vibrator was switched and (2) the hydraulic shock wave could effectively improve the excitation force of the system. The excitation force increased with an increase in the oil supply pressure, spindle speed, and load. However, it was negatively correlated with the spring stiffness. The amplitude of the vibration waveform output was positively correlated with the oil supply pressure and negatively correlated with the spindle speed and load. The amplitude first increased and then decreased as the stiffness of the vibration spring increased. The only influence of the precompressed length of the spring on the system output was its alteration of the vibration center of the system output vibration.

1. Introduction

Hydraulic excitation is the most common technical application of the pulsating flow hydraulic theory. It involves the transformation of the pressure energy of a liquid into the reciprocating vibration kinetic energy of a piston by converting the direct-current liquid flow into an alternating-current liquid flow [1]. Hydraulic excitation has unique advantages compared with the other two types of vibration technologies (i.e., mechanical vibration caused by centrifugal force [2] and electromagnetic vibration excited by the Lorentz force [3]). These include high output power, convenient adjustment of output characteristics, reliable operation, and suitability to special working environments. It is widely used in construction, mining, aerospace, and other engineering fields [4–7].

A hydraulic vibrator is the core functional component for generating an alternating pressure flow in hydraulic excitation systems. It can be categorized as forced distribution or feedback distribution, based on the feedback relationship between the piston and vibrator. The former has a relatively simple structure and control mechanism and is applied widely. It controls the alternating fluid flow required by the piston vibration by driving the valve core with an external element. Therefore, the output characteristics of the vibration system depend stringently on the dynamic characteristics of the external driving element [8]. Prior to 2006, most hydraulic vibrators used a slide-valve structure. That is, the valve core would undergo periodic reciprocating linear motion during an excitation. However, with an increase in the excitation frequency, the driving force required for the reciprocating movement of the valve core increases, and the

dynamic response of an ordinary external driving element cannot satisfy the system requirements. The output of the excitation system is unstable, and the waveform is distorted severely. This results in bandwidth limitation of the excitation system (<50 Hz) [9, 10]. Considering this deficiency, MTS Company, U.S.A., proposed a multistage electric feedback servo valve driven by a voice coil motor. Its effective excitation frequency could attain 1000 Hz. However, it was limited by a low output force of the voice coil motor [11].

With the recent advances in complex and expensive driving components, researchers have opted to improve the structure of the valve core and study its working characteristics. A common method involves the rotation of the valve structure and realization of oil circuit switching through a constant rotation of the valve element. Joseph [12] designed a plug-type hydraulic rotary valve with a movable seat, which permitted a maximum working pressure of 60 MPa and a maximum frequency of 2000 Hz. Sallas [13] designed a rotary servo valve with a low inertia by using a hollow valve spool structure. Collins [14] designed a special-shaped valve spool with a variable equivalent diameter. The dynamics of multiple pairs of flow orifices could offset the hydraulic pressure and balance the nonuniform axial force on the rotary valve. This eliminated the disadvantage of insufficient high-pressure working conditions owing to the "Bernoulli effect." Wang et al. [15–17] also investigated the flow torque on a rotary valve spool. They studied the flow characteristics of a four-way rotary valve spool with different orifice shapes and proposed a corresponding optimized design scheme for flow force compensation. They also studied the total distortion of the output waveform of the vibrator based on the total harmonic distortion (THD) theory. To solve the problem of interference between the operating frequency and output amplitude of the rotary valve, Ruan et al. [18, 19] proposed an innovative rotary vibrator with two degrees of freedom. It could separately adjust the frequency and amplitude of the vibration output of the hydraulic cylinder by controlling the rotation speed of the spool and its axial displacement. Subsequently, they achieved a reasonable control of the vibration output offset through a common rotary servo valve connected in parallel with the original vibrator. Consequently, they realized the separation control of the amplitude, frequency, and offset of the output amplitude of the rotary vibrator [20–22].

The flow area of the working throttle port varies throughout the working process of the aforementioned hydraulic vibrator, and its maximum value is relatively marginal. That is, the alternating fluid flow required by the excitation system is the gap flow output from the throttle port of the vibrator, which causes significant pressure loss and severe cavitation at the valve port. This may result in the failure of the valve port structure of the vibrator owing to heat and cavitation under the conditions of high frequency, high pressure, and large flow rate. It also causes a certain amount of energy waste in the system [15, 23–27]. In addition, the opening and closing of the valve port and abrupt variation in the actuator motion state in the hydraulic system cause a hydraulic shock. At this time, the flow rate and pressure of the liquid in the system pipeline produce severe pulsation. That is, a pressure transient flow occurs in the pipeline, which would severely affect the working characteristics of the hydraulic system [28]. However, most researchers omit the presence of pressured transient flow in the pipeline while modeling hydraulic excitation systems [18, 20]. This may affect the accuracy of the output parameters.

When a hydraulic shock occurs, the maximum pressure is approximately 1.5–5 times the steady-state pressure. Moreover, the propagation speed of the shock wave in the pipeline (at 800–1200 m/s) and the energy of the hydraulic shock wave are significantly high. Therefore, for a general hydraulic system, hydraulic shocks are hazardous and should be eliminated or mitigated [29]. However, the pressure wave can be favorable if it can be controlled actively using a hydraulic excitation system and its large amount of energy used for the vibration output [30, 31]. Thus, in this study, a high-flow hydraulic impact rotary vibrator with a vertical differential hydraulic vibration system is proposed, considering its flow distribution function. It is based on the mechanism of hydraulic impact. This innovative vibrator adopts a multilayer valve sleeve structure. This structure significantly increases the vibrator's maximum flow area and the proportion of the limit opening area of the working throttle port in a working cycle. This satisfies the requirements of large flow conditions and simultaneously improves the gradient of flow area variation. Thus, it minimizes the throttling loss of the vibration exciter, enhances the hydraulic impact effect of the vibration-excitation system, and improves the exciting force of the system.

This paper is organized as follows. Section 2 introduces the structural characteristics of the hydraulic impact rotary vibrator and the working principle of the hydraulic vibration-excitation system with the vibrator as the flow distribution element. In Section 3, numerical models of the excitation system (both without and with the pipeline effect) are established. Section 4 introduces the experimental apparatus used to verify the effectiveness of the excitation system model. In Section 5, an analysis of the following two aspects is presented: (1) the output characteristics of the hydraulic system while switching the working state of the vibrator and (2) the influence of different system parameters on the displacement and exciting force of the exciting system. Finally, Section 6 presents the conclusions.

2. Proposed Vibration-Excitation System

2.1. Working Principle. Figure 1(a) shows a schematic of the proposed hydraulic vibration-excitation system. Here, a differential cylinder is fixed vertically on a frame. Furthermore, the excited mass body connects a piston rod with a rigid connection. The hydraulic power pack of the system comprises a manually regulated fixed-displacement axial piston pump and an overflow valve. The hydraulic exciter is connected to a low-power frequency conversion motor through a coupling. The coupling can alter the direction of the internal oil circuit of the vibrator, thereby varying the

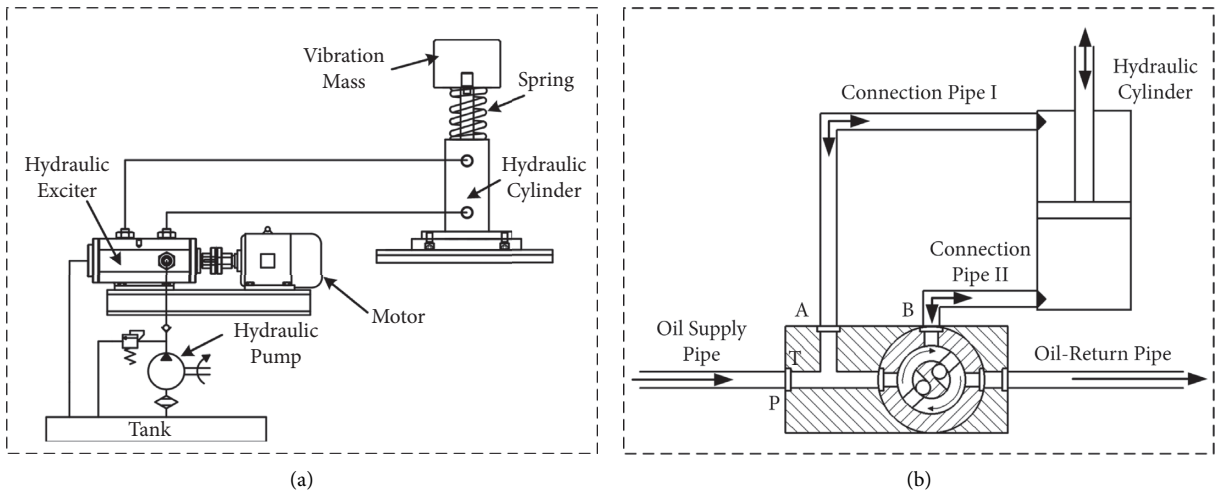

Figure 1: (a) Hydraulic vibration-excitation system and (b) its working principle.

pressure of the hydraulic cylinder and realizing the vibration output.

As shown in Figure 1(b), the motor drives the rotor shaft inside the vibrator to rotate at a preset angular speed. When it rotates to a certain angle range, oil port P is connected to oil port B, and the system is in the differential connection state (see Figure 2(a)). The piston rod moves upward owing to the asymmetry in the areas of the two cavities in the hydraulic cylinder. When oil port B is connected to oil port T, the system presents an oil-return state (see Figure 2(b)). The pressure at the rear end of the cylinder is reduced instantaneously, which causes the piston rod to move downward rapidly. To complete the above working cycle, the structural design of the vibrator ensures that oil ports P and T cannot be connected to oil port B simultaneously. It is noteworthy that the conversion process may cause a hydraulic impact in the two cavities of the hydraulic cylinder when the vibrator reversing speed is sufficiently high. Moreover, the flow gain is improved by optimizing the orifice area.

The originally designed hydraulic vibrator is the core element of the vibration-excitation system. It mainly comprises a hollow spindle, an inner stator sleeve, an external stator sleeve, and a flow stop (see Figure 2). Actuator port A connects to the rod cavity of the differential cylinder, whereas actuator port B connects to another cavity. The step groove on the left side of the hollow spindle ensures permanent communication between actuator port A and oil inlet P during the rotation. Meanwhile, six nonpenetrating trapezoidal slots are arranged uniformly along the circumference of the hollow spindle and are spaced into two groups. The groove bottom of each group of grooves has a through hole with an area less than half that of the groove bottom. Two sets of long oil holes are arranged with the center face of the flow stop as the center of symmetry. With the rotation of the hollow spindle, the two sets of oil holes would communicate alternately with actuator port B. The flow stop prevents the two sets of oil holes from connecting with actuator port B simultaneously.

2.2. Variable Orifice Area of the Hydraulic Vibrator. To reduce the throttle loss of the vibrator in the working process and increase its flow gain, the throttling should be shortened as much as possible and an adequate flow area should be ensured. Therefore, a liquid storage tank is machined on the inner stator sleeve, which is a long groove equal in size to the trapezoidal groove on the hollow spindle. There is a through hole at the bottom of the groove with an equal interval between the two trapezoidal grooves on the hollow spindle. It functions as a throttle. The coordination between the inner stator sleeve and hollow spindle of the vibrator under the two working conditions is shown in Figures 3(a) and 3(b), and Figure 3(c) shows the radial section diagram of the vibrator at the throttle. The shaded part of Figure 3(d) shows the shielding area when the orifice is not fully open.

Here, R is the radius of the hollow spindle, N is the number of grooves (always even), r is the radius of the semicircle at both ends of the throttle, and L is the length of the throttle orifice. Thus, the angle of rotation required for the orifice from being fully closed to being fully open is $2\arcsin(r/R)$. The throttle is approximately rectangular with a length and width of l and 2r, respectively. The flow area of the orifice of the vibrator during its rotation is calculated as follows:

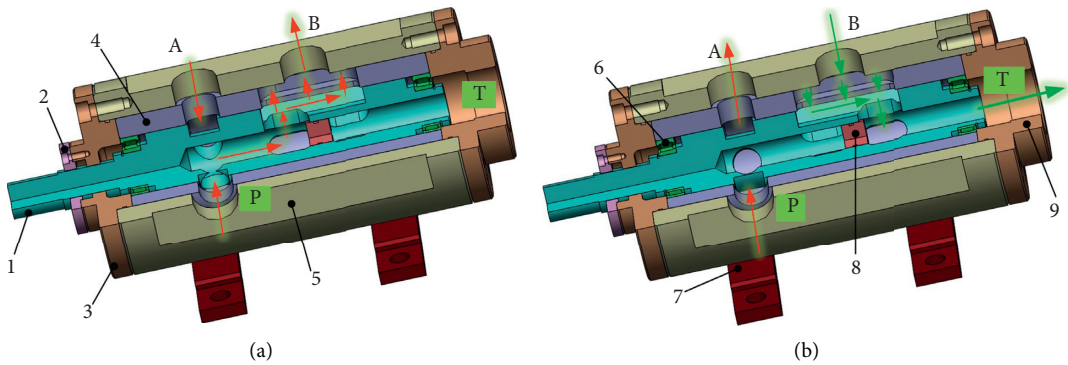

Figure 2: Hydraulic shock rotary vibrator. (a) Differential connection state. (b) Oil-return connection state. 1, hollow spindle; 2, sealing cover; 3, front end cap; 4, inner stator sleeve; 5, external stator sleeve; 6, bearing; 7, base support; 8, flow stop; and 9, rear end cap. A: port connected to the rod side of the cylinder; B: port connected to the head side of the cylinder; P: supply oil port; and T: oil-return port.

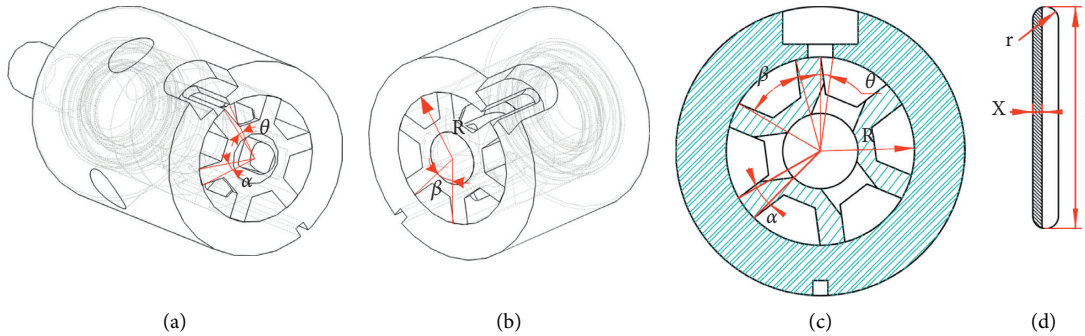

Figure 3: (a) Profile of hydraulic vibrator in differential connection state. (b) Its connection with the tank. (c) Section diagram of the valve. (d) Flow area.

$$A_v = \begin{cases} 2LR\sin\left(\dfrac{\theta}{2} - \dfrac{k\pi}{N}\right), & \dfrac{2k\pi}{N} \le \theta < \dfrac{2k\pi}{N} + 2\arcsin\left(\dfrac{r}{R}\right), \\ 2Lr, & \dfrac{2k\pi}{N} + 2\arcsin\left(\dfrac{r}{R}\right) \le \theta < \dfrac{2(k+1)\pi}{N} - 2\arcsin\left(\dfrac{r}{R}\right), \\ 2LR\sin\left[\dfrac{(k+1)\pi}{N} - \dfrac{\theta}{2}\right], & \dfrac{2(k+1)\pi}{N} - 2\arcsin\left(\dfrac{r}{R}\right) \le \theta < \dfrac{2(k+1)\pi}{N}, \end{cases} \quad (1)$$

where $k = 0, 1, 2, 3, \ldots$, and when k is odd, the vibrator maintains the vibration-excitation system in the differential connection state. When k is even, the cap end of the differential hydraulic cylinder is connected to the oil tank. The flow area variation rule of the throttle orifice of the hydraulic vibrator used in the hydraulic excitation system in this study is shown in Figure 4. As can be observed, when the spindle rotates once, the orifice area varies six times alternately, and three excitation cycles can be completed. The opening and closing time of the orifice is shorter than the time occupied by the limit opening, and a larger variation in the through-flow area can be completed in a shorter time to obtain a higher flow gain.

A linear relationship exists between the rotation angle (θ) of the vibrator spindle and its rotation speed (N_s) at time t:

$$\theta = \frac{2\pi N_r t}{60}. \quad (2)$$

3. System Model

The hydraulic excitation system can be regarded as a hydraulic power mechanism comprising a two-position three-way valve and a vertical asymmetric oil cylinder.

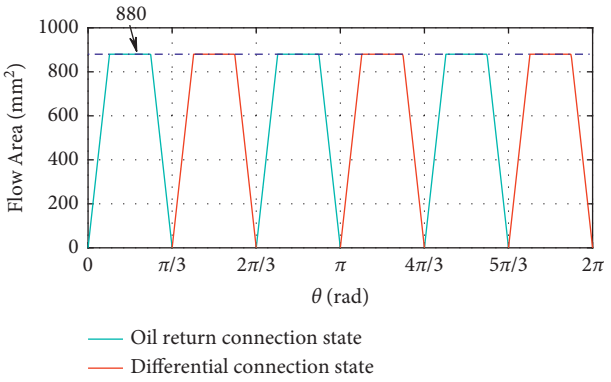

Figure 4: Flow area of the throttle port.

Furthermore, the load is a single-degree-of-freedom system composed of mass and spring elements. To simplify the analysis, the following assumptions should be made regarding the system:

(1) The geometric size of the rotary vibrator has no machining error, radial clearance, or leakage.

(2) The oil supply pressure remains unaltered.

A simplified schematic of the system is shown in Figure 5(a). Here, the zero position of piston displacement (y_p) is specified as the lowest permissible position of the cylinder stroke (l_{s0}). Furthermore, the upward movement of the piston is forward. When the system starts, the exciter is in a differential connection state, the initial value of the piston displacement is $l_{s0}/2$, and the precompression length of the spring is D_p.

3.1. System Model without Pipeline Effect. A hydraulic bridge (see Figure 5(b)) can be established if the influence of pressure and flow pulsation in the pipeline of the hydraulic circuit of the excitation system is omitted. Here,

$$p_2 = p_s. \tag{3}$$

According to the orifice flow formula, the static characteristic equation of the system can be obtained as follows:

$$Q_L = aC_dA_v\sqrt{\frac{2(bp_s - ap_1 - cp_t)}{\rho}}, \tag{4}$$

where C_d is the flow coefficient of the throttle, Q_L is the load flow of the system, and ρ is the density of oil. a, b, and c are conditional coefficients:

$$\begin{cases} a = -1, \quad b = 0, \quad c = 1, \quad \text{when } k \text{ is even}, \\ a = 1, \quad b = 1, \quad c = 0, \quad \text{when } k \text{ is odd}. \end{cases} \tag{5}$$

According to the flow continuity theorem, the flow continuity equations of the two cavities of the hydraulic cylinders are as follows:

$$\begin{cases} Q_1 = A_1\dfrac{dy_p}{dt} + \dfrac{A_1y_p}{K}\dfrac{dp_1}{dt} + C_i(p_2 - p_1), \\ Q_2 = A_2\dfrac{dy_p}{dt} + \dfrac{A_2(l_{s0-}y_p)}{K}\dfrac{dp_2}{dt} + C_i(p_2 - p_1) + C_ep_2, \end{cases} \tag{6}$$

where K is the bulk modulus of oil.

The rear end of the differential cylinder is its control cavity. Hence,

$$Q_L = Q_1. \tag{7}$$

The force balance equation is obtained as follows by analyzing the dynamic process of the vertical differential hydraulic cylinder:

$$M\frac{d^2y_p}{dt^2} = A_1p_1 - A_2p_2 - B_p\dot{y}_p - Mg + k_s\left(\frac{l_{s0}}{2} + D_p - y_p\right), \tag{8}$$

where B_p is the viscous friction coefficient of moving parts such as the hydraulic cylinder piston and load and k_s is the stiffness coefficient of the vibration spring.

The piston displacement, its first derivative, and the pressure of the rear end of the cylinder are selected as the state variables. That is,

$$\begin{aligned} x &= [x_1, x_2, x_3]^T \\ &= [y_p, \dot{y_p}, p_1]^T. \end{aligned} \tag{9}$$

Combining equations (4)–(9), we obtain the state equation of the excitation system without the pipeline effect as

$$\begin{cases} \dot{x_1} = x_2, \\ \dot{x_2} = -\dfrac{k_s}{M}x_1 - \dfrac{B_p}{M}x_2 + \dfrac{A_1}{M}x_3 - \dfrac{A_2}{M}p_s + \dfrac{k_s}{M}(l_{s0} + D_p) - g, \\ \dot{x_3} = \dfrac{aC_dA_vK}{A_1x_1}\sqrt{\dfrac{2(bp_s - ax_1 - cp_t)}{\rho}} - \dfrac{K}{x_1}x_2 - \dfrac{C_iK}{A_1x_1}(p_s - x_3). \end{cases} \tag{10}$$

Assuming that $\mathbf{y}$ is the output variable of this model,

$$\begin{aligned} \mathbf{y} &= [y_1, y_2, y_3]^T \\ &= [y_p, \dot{y_p}, F]^T, \end{aligned} \tag{11}$$

where F is the exciting force output by the system. Furthermore,

$$F = A_1p_1 - A_2p_2. \tag{12}$$

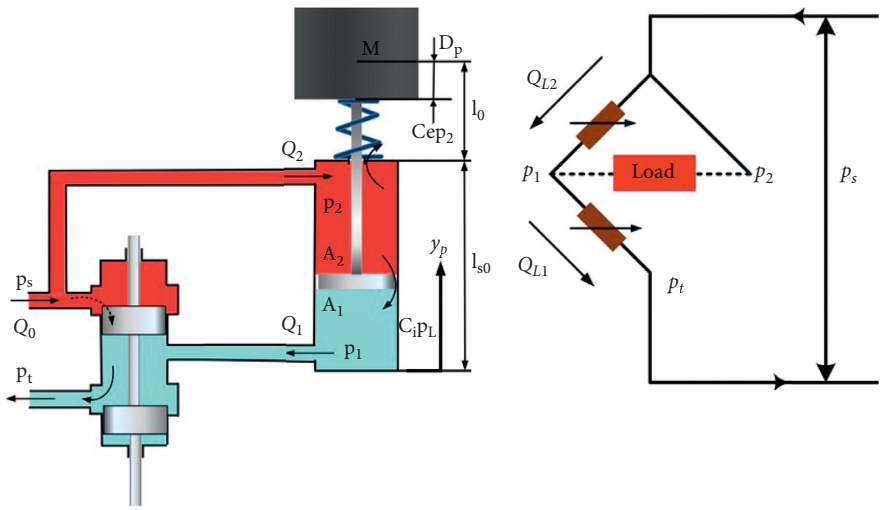

(a) (b)

Figure 5: (a) Simplified system schematic diagram and (b) equivalent hydraulic bridge diagram of the system without pipeline effect.

3.2. System Model with Pipeline Effect

3.2.1. Model for Calculating Transient Flow of the Pressurized Pipeline. Based on the mechanism of hydraulic shock and considering that the throttle port of the hydraulic vibrator opens and closes rapidly when its hollow spindle rotates at a high speed, the pressure and flow rate of oil in the hydraulic pipeline connected with the vibrator would vary dramatically. That is, a pressure transient flow would be formed. Thus, the transient flow calculation model of the pressure pipeline can be established by considering the transient variation in the oil state in the pipeline caused by events such as the valve closure.

Based on Figure 6, a force analysis is conducted on the fluid microelement section of the pressure pipeline. Sections B and C are perpendicular to the tube axis, which forms an angle α with the horizontal. The distance between the two cross sections is dx. The area, diameter, and center-point height of section B are A, D, and Z, respectively. At this position, the water head is H, Q is the flow rate in the pipeline, τ_0 is the frictional resistance of the pipeline, and f is the Darcy frictional resistance coefficient of the tube.

To facilitate modeling and analysis of the complete system, the water head is converted into an equivalent pressure:

$$H = \frac{p}{\rho g} + Z. \tag{13}$$

Its equation of motion is established by Newton's second law:

$$\frac{\partial p}{\partial x} - \rho g \sin\alpha + \frac{\rho}{A}\left(A\frac{\partial v}{\partial t} + Q\frac{\partial Q}{\partial x}\right) + \frac{\pi D\tau_0}{A} = 0. \tag{14}$$

Assuming that the frictional coefficient remains constant during transient flow and is equal to that of the steady flow, it can be obtained by Darcy's formula as

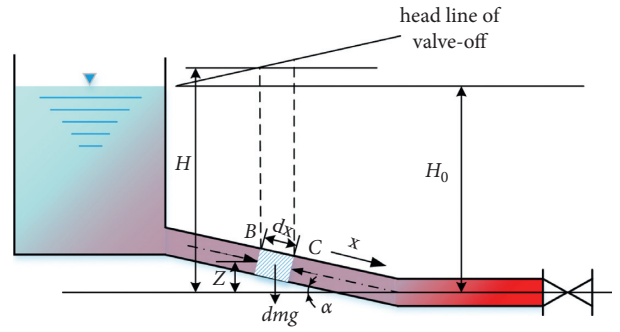

Figure 6: Physical model of pressurized transient flow.

$$\tau_0 = \frac{\rho f Q|Q|}{8A^2}. \tag{15}$$

The equation of motion in the pressurized transient flow pipeline is obtained as follows by substituting equation (15) in equation (14), considering that the temporal derivative of fluid velocity is significantly larger than the spatial derivative, and omitting the pressure variations caused by the differences in terrain elevation:

$$\frac{\partial p}{\partial x} + \frac{\rho}{A}\frac{\partial Q}{\partial t} + \frac{\rho f Q|Q|}{2DA^2} = 0. \tag{16}$$

From the law of conservation of mass, the continuity equation of the transient flow of the aforementioned microelement segment in the period t is

$$\frac{\partial p}{\partial t} + \frac{c^2\rho}{A}\frac{\partial Q}{\partial x} = 0, \tag{17}$$

where c is the wave velocity of the water hammer. It is expressed as follows according to the theory of elastic water hammer:

$$c = \frac{1}{\sqrt{\rho\left((1/A)(\mathrm{d}A/\mathrm{d}p) + (1/\rho)(\mathrm{d}\rho/\mathrm{d}p)\right)}}. \tag{18}$$

Equations (16) and (17) together constitute the basic calculation model of the transient flow in the pressurized pipeline.

3.2.2. System Simulation Model with Pipeline Effect. When the pipeline effect of the system during the excitation process is considered, it is necessary to establish a transient flow calculation model for all the pressurized pipelines connected to the exciter. However, the pipeline connection state is different. Moreover, the boundary conditions are complex under different working conditions of the vibration exciter, which hinders the modeling process. SimulationX provides researchers with a multidisciplinary system dynamics simulation platform that can be oriented to the physical object model. Various physical components can be modified and developed through its open and editable component library. Furthermore, the external solver based on the backward differentiation formula (BDF) or other custom algorithms can realize the transient simulation solution of the system-state equations in the time domain.

The simulation model shown in Figure 7 was established for the hydraulic vibration system. The core issue in this model is the development of a new type of hydraulic vibrator. Based on the communication of the hydraulic circuit in the two working states of the vibrator, it is equivalent to an initial oil circuit with an H-shaped structure. A throttle valve with an adjustable flow area is added to two branch oil paths connected to working oil port B. Furthermore, the variation in the flow area is established according to the throttle area model. The two operating conditions are switched by time-sharing control at intervals of $T/2$. The throttle valve opening area is controlled by four functions: *curve function*, *function signal*, *three-point function*, and *pulse generator*.

Based on equation (2), the *curve function* can be used to simulate the rotation angle of the spool within time t:

$$\gamma = \frac{2\pi N_s}{60} \times t. \tag{19}$$

The *function signal* is used to carry out the remainder of the calculation of the rotating angle of the spool with $2\pi/N$ as the reference interval. The *three-point function* calculates the remainder in sections as

$$f_\delta = \begin{cases} 2LR\ \sin\left(\dfrac{\delta}{2}\right), & \\ 0 \le \delta < 2\mathrm{arc}\sin\left(\dfrac{r}{R}\right), & \\ 2Lr, & \\ 2\mathrm{arc}\sin\left(\dfrac{r}{R}\right) \le \delta < \dfrac{2\pi}{N} - 2\mathrm{arc}\sin\left(\dfrac{r}{R}\right), & \\ 2LR\ \sin\left[\dfrac{\pi}{N} - \dfrac{\delta}{2}\right], & \\ \dfrac{2(k+1)\pi}{N} - 2\mathrm{arc\,in}\left(\dfrac{r}{R}\right) \le \delta < \dfrac{2\pi}{N}, & \end{cases} \tag{20}$$

where δ is the angle of function mod calculation and solution.

The *pulse generator* uses a trapezoidal function to calculate f_δ at intervals of $T/2$ and assigns it to the flow area of the throttle valve in the two oil circuits. Thus, it connects the cap end of the hydraulic cylinder with a phase difference of $T/2$. T is the time required for the spool to rotate by $4\pi/N$ (rad).

$$T = \frac{120}{N \times N_s}. \tag{21}$$

Other oil circuits of the vibrator are equivalent to a T-junction and a 90° elbow connection with corresponding geometric dimensions. In the simulations, owing to the need to consider the influence of the pressure fluctuation effect on the characteristics of the excitation system, the internal pipelines of the vibrator and the pipelines connected with the double chamber of the hydraulic cylinder are established as a distributed line model, which is based on the pressure fluctuation calculation used by the finite volume method (FVM) in time-domain transient simulations.

The computational model of the transient flow in the

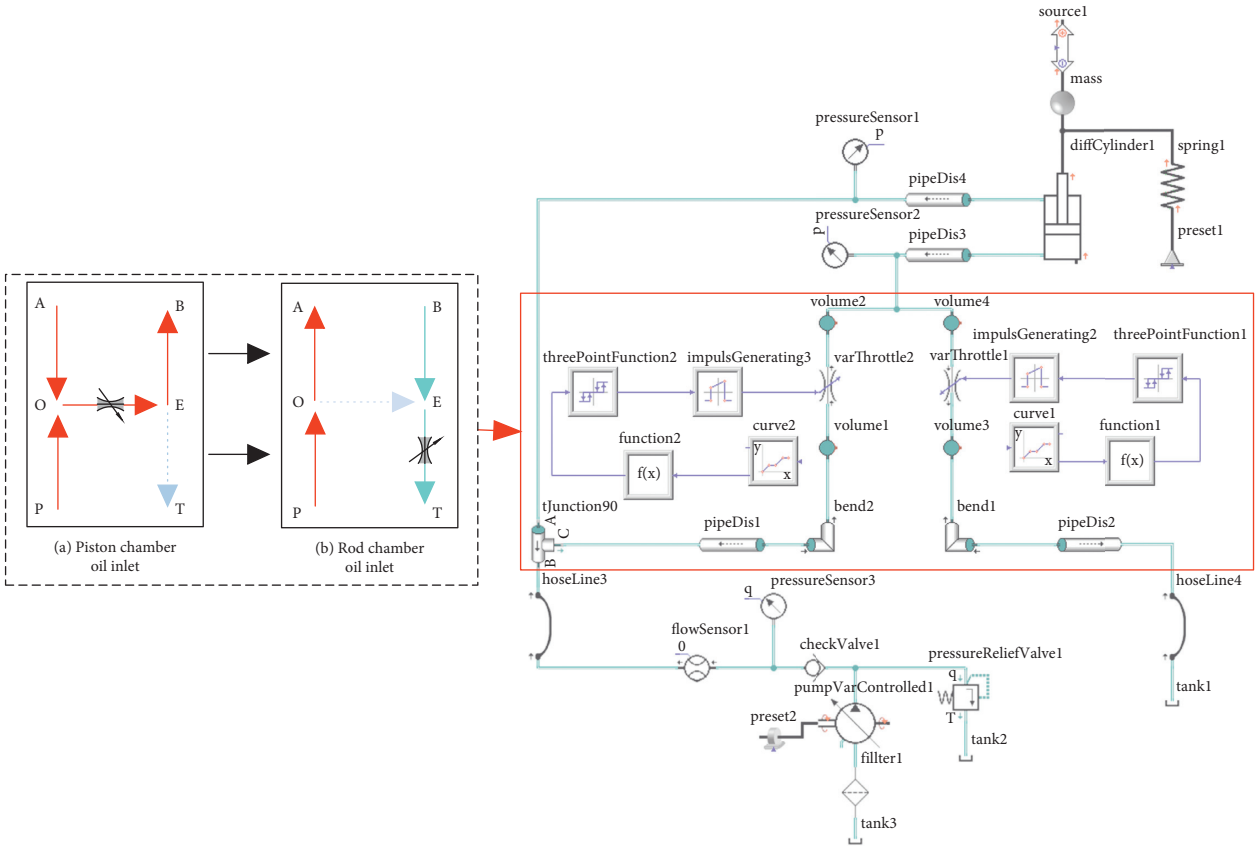

Figure 7: SimulationX model of the vibration-excitation system.

pressure pipeline comprises two quasilinear hyperbolic partial differential equations. Furthermore, its analytical solution cannot be obtained directly. The FVM can discretize the solution domain into discrete grids of finite size and solve the above computational model via integration in each control volume. Because the two variables in the calculation model are related to the position and time, it is necessary to carry out a discrete analysis of the control body nodes and time. The discretization for this analysis is shown in Figure 8. The transient flow can be integrated from t to $t + \Delta t$ in a control volume, as follows:

$$\begin{cases} \int_t^{t+\Delta t} \int_{\Delta V} \frac{\partial p}{\partial x} \mathrm{d}V\mathrm{d}t + \frac{\rho}{A} \int_t^{t+\Delta t} \int_{\Delta V} \frac{\partial Q}{\partial t} \mathrm{d}V\mathrm{d}t + \int_t^{t+\Delta t} \int_{\Delta V} \frac{\rho f Q|Q|}{2DA^2} \mathrm{d}V\mathrm{d}t = 0, \\ \frac{c^2\rho}{A} \int_t^{t+\Delta t} \int_{\Delta V} \frac{\partial Q}{\partial x} \mathrm{d}V\mathrm{d}t + \int_t^{t+\Delta t} \int_{\Delta V} \frac{\partial p}{\partial t} \mathrm{d}V\mathrm{d}t = 0. \end{cases} \tag{22}$$

Using the Gauss formula, the plane parallel to the pipeline cross section is passed through discrete nodes in the control volume. In addition, the integral in equation (22) is transformed into an area fraction of the cross section perpendicular to the volume flow in the corresponding control volume.

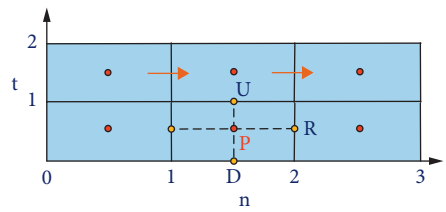

Figure 8: Illustration of finite volume method.

$$\begin{cases} \int_t^{t+\Delta t}\left(\int_A \vec{n}p\mathrm{d}A\right)\mathrm{d}t + \dfrac{\rho}{A}\int_{\Delta V}\left(\int_t^{t+\Delta t}\dfrac{\partial Q}{\partial t}\mathrm{d}t\right)\mathrm{d}V \\ +\int_{\Delta V}\left(\int_t^{t+\Delta t}\dfrac{\rho f Q|Q|}{2DA^2}\mathrm{d}t\right)\mathrm{d}V = 0, \\ \dfrac{c^2\rho}{A}\int_t^{t+\Delta t}\left(\int_A \vec{n}Q\ dA\right)\mathrm{d}t + \int_{\Delta V}\left(\int_t^{t+\Delta t}\dfrac{\partial p}{\partial t}\mathrm{d}t\right)\mathrm{d}V = 0, \end{cases} \tag{23}$$

where $\Delta V = A\Delta x$.

Here, ΔV is the discrete control volume, $\vec{n}$ is the unit vector in the normal direction outside the cross-sectional area of the control volume, and A is the cross-sectional area of the control volume.

$$\begin{cases} \vec{n}p = p_R - p_L \approx \dfrac{p_2^1 + p_2^0}{2} - \dfrac{p_1^1 + p_1^0}{2}, \\ \vec{n}Q = Q_R - Q_L \approx \dfrac{Q_2^1 + Q_2^0}{2} - \dfrac{Q_1^1 + Q_1^0}{2}, \\ \dfrac{\partial Q}{\partial t} \approx \dfrac{Q_U - Q_D}{\Delta t} \approx \dfrac{Q_2^1 + Q_1^1}{2\Delta t} - \dfrac{Q_2^0 + Q_1^0}{2\Delta t}, \\ \dfrac{\partial p}{\partial t} \approx \dfrac{p_U - p_D}{\Delta t} \approx \dfrac{p_2^1 + p_1^1}{2\Delta t} - \dfrac{p_2^0 + p_1^0}{2\Delta t}. \end{cases} \tag{24}$$

The friction term can be obtained in a semiimplicit form, as follows:

$$\frac{\rho f Q|Q|}{2DA^2} = \frac{\rho f\left(Q_1^1 + Q_2^1\right)\left|Q_1^0 + Q_2^0\right|}{4DA^2}. \tag{25}$$

A discrete form of the transient flow calculation model of the pressure pipeline can be obtained as follows by substituting equations (24) and (25) into equation (22):

$$\begin{cases} \dfrac{A\Delta t}{2}\left[\left(p_2^1 + p_2^0\right) - \left(p_1^1 + p_1^0\right)\right] + \dfrac{\rho\Delta x}{2A}\left[\left(Q_2^1 + Q_1^1\right) - \left(Q_2^0 + Q_1^0\right)\right] \\ +\dfrac{\rho f\Delta t\Delta x}{4\ DA}\left(Q_1^1 + Q_2^1\right)\left|Q_1^0 + Q_2^0\right| = 0, \\ \dfrac{c^2\rho\Delta t}{2}\left[\left(Q_2^1 + Q_2^0\right) - \left(Q_1^1 + Q_1^0\right)\right] + \left[\left(p_2^1 + p_1^1\right) - \left(p_2^0 + p_1^0\right)\right] = 0. \end{cases} \tag{26}$$

Finally, a global calculation model of the excitation system is established based on the boundary conditions and initial state set by the SimulationX platform. It can solve the regulation law of the transient pressure of the pressurized pipeline, as well as the upper and lower chambers of the hydraulic cylinder under different working conditions. The key geometric parameters of the components used in the simulation model are set according to the real parameters of the physical experimental platform.

4. Experimental Apparatus

The experimental apparatus for the vibration-excitation system is shown in Figure 9(a), and its schematic diagram is shown in Figure 9(b). The spindle of the rotary vibration exciter was connected rigidly to a three-phase asynchronous motor through a coupling. The closing position of the throttle port was defined as its initial position, and the machining position of the keyway was considered as the marking point of the initial position. The vibration actuator comprised a vertical differential cylinder and a variable mass loading mechanism. The precompressed length of the vibration spring could be adjusted via the nut lock on the piston rod so that a vibration test with a variable load and a variable precompressed length of spring could be conducted.

In addition, a Siemens V 20 frequency converter was connected in series with the input end of the three-phase asynchronous motor to control the output speed of the motor and adjust the angular rotational speed of the spindle of the vibrator. Hence, the formula for the vibrator shaft speed (N_s) is

$$N_s = \frac{n}{50} \times N_r, \tag{27}$$

where N_r is the rated speed of the motor and n is the set value for the frequency converter.

In this experimental setup, the sensors for oil pressure and flow were installed at the outlet of the pump station, oil ports of the two cavities of the hydraulic cylinder, and working oil port of the hydraulic vibration exciter. Moreover, an ICP acceleration sensor was installed on the horizontal end face of the loading mechanism to detect the acceleration of the piston. The monitoring signals of all the sensors were finally collected by a COINV-INV 3018 CT 24 bit high-precision data collector and transmitted to a computer. The data acquisition and signal processing (DASP) system installed on the computer can perform the corresponding frequency-domain integration operation on vibration acceleration signals and conveniently and effectively obtain the vibration waveform, frequency, amplitude, instantaneous velocity, and other parameters (see Table 1 for other key parameters of the physical experimental setup).

5. Results and Analysis

5.1. Model Validity. The two system models detailed in Section 3 were solved and compared with the corresponding experimental results from the excitation system to verify the effectiveness of the two models. The settings for the system variable parameters are listed in Table 2.

Figures 10(a)–10(c), respectively, depict comparison of the system output displacements, velocities, and exciting forces computed using the two models with the experimental measurements under different parameter settings. The results obtained using the two models were consistent with the experimental results. However, a comparison of the variation trends of the output parameters of the two models in a cycle revealed that the results of the system model that incorporated the pipeline effect agreed better with the experimental results than those of the system without the pipeline effect. This was because the fluid pressure in all the chambers in the excitation system (e.g., the two cavities of the hydraulic cylinder and all the pipelines) varied significantly with the high-frequency variation of the vibrator throttle. However, in the model without the pipeline effect, the transient pressure in the hydraulic system (e.g., the liquid pressure in the cylinder rod cavity) was omitted. It was consistently equal to the supply pressure of the system. Its omission from the calculations would also result in a significant error in the system output. In Table 3, the differences in characteristic physical quantities of output waveform between the experimental system and each of the two models are listed. Here, the error ratio is referred to as the ratio of the absolute difference between the result obtained using the corresponding system model and the physical experimental result to the physical experimental result. In Figure 11(c), the excitation force in a period as measured by the models and experiment is compared and analyzed. Although the overall error between the model without the pipeline effect and the experimental results is large, their variation trends were essentially consistent in interval AB. Therefore, it can be concluded that the transient pressure in this interval had a negligible effect on the excitation force of the system output. In contrast, in interval BC, the excitation force output by the system was determined mainly by the transient pressure in the system. When the pipeline effect was not considered, it resulted in a large error in the model results. That is, the excitation force output consisted of two parts: a hydrostatic transmission based on the system and a hydraulic impact force caused by the transient flow in the system cavities. To facilitate further analysis, the exciting forces of these two parts were defined as the foundation excitation force and impact exciting force, respectively.

A relatively marginal error was also present in the result from the model with the pipeline effect. It could be owing to unavoidable problems, such as volume losses of the pump station in the experiment. The error resulted in an insufficient supply of liquid under the corresponding conditions. The above analysis demonstrates that the model with the pipeline effect was more accurate.

5.2. Effect of Switching the Oil Circuit on the Excitation System. By analyzing the variation in the displacement and velocity curves of the excitation system with the orifice area of the vibrator shown in Figure 11(a), it can be concluded that the excitation frequency of the system was consistent with the rotational frequency of the rotating spindle of the hydraulic vibrator. After the vibrator completed a period of rotation, the system could achieve a stable vibration from its initial state with good transient response characteristics. When the hydraulic vibrator was switched from the oil-return state to the differential state, the velocity varied significantly from a negative value to approximately zero. Next, the excited object realized a reverse movement from the downward to the upward direction. However, when the vibrator transformed from the differential state to the oil-return state, the velocity rapidly varied from forward maximum to reverse

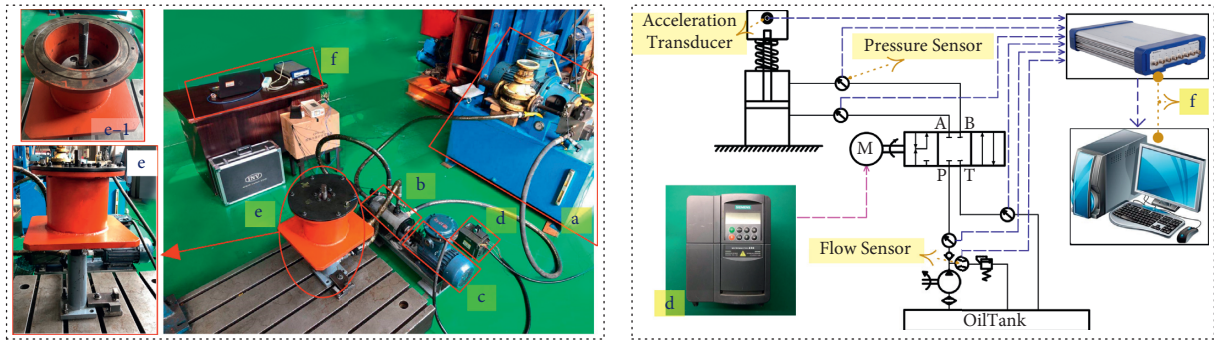

(a) (b)

Figure 9: Experimental apparatus (a) and its schematic diagram (b). (A) Hydraulic power supply, (B) hydraulic shock rotary vibrator, (C) three-phase asynchronous motor, (D) Siemens V20 inverter, (E) vibration actuator, (E-1) load mechanism with variable mass, and (F) data acquisition and signal analyzer.

Table 1: Key parameters of the hydraulic vibration-excitation system.

Parameter	Value	Unit
Cylinder diameter	63	mm
Rod diameter	35	mm
Stroke of cylinder	100	mm
Length of oil supply pipe	2000	mm
Length of oil-return pipe	2000	mm
Length of connection pipe I	800	mm
Length of connection pipe II	1200	mm
Inner diameter of oil supply pipe and connection pipe I	22	mm
Inner diameter of oil-return pipe and connection pipe II	32	mm
Rate speed of motor	1440	r/min
Spring stiffness	180000	N/m
N	6	—

Table 2: Settings for the variable parameters of the hydraulic vibration-excitation system.

Parameter	Value	Unit
Oil supply pressure	5	MPa
Spindle speed (set value of frequency converter)	316.8 (11)	r/min (/)
Load	100	kg
Spring stiffness	180000	N/m
Precompressed spring length	2	cm

maximum at a high rate. Moreover, the downward movement velocity was reduced gradually. Because the area of the orifice was at its maximum value for a long time, it again increased the velocity of the downward movement. However, it was significantly lower than that at the instant of switching. Therefore, the hydraulic vibrator had a positive effect on the completion of vibration commutation.

As shown in Figures 11(b) and 11(d), the influence of the pipeline effect on the hydraulic system resulted in a difference in pressure fluctuation amplitude between the two cavities of the hydraulic cylinder. This caused marginal fluctuations in the output force. When the vibrator abruptly turned on the oil circuit, it abruptly transformed the hydraulic cylinder into a differential connection state. This implies that the oil flow from the head end of the hydraulic cylinder to the oil tank was abruptly cut off and connected with the rod end, which caused the pressure of the two cavities of the hydraulic cylinder to increase abruptly to approximately 8 MPa. As the throttle port opened further, the two chambers interacted at a pressure marginally higher than the oil supply pressure (5 MPa). This pushed out the piston rod of the hydraulic cylinder. When the head end of the hydraulic cylinder was connected abruptly to the oil tank, the circuit capable of discharging high-pressure oil at the rod end of the hydraulic cylinder closed abruptly. This resulted in an instantaneous surge in its pressure to 12 MPa, which was more than twice the system pressure. At this point, the pressure in the lower chamber was minimized instantaneously. In addition, the system generated the maximum exciting force of the entire vibration cycle (approximately 26 kN). However, owing to the instantaneous increase in the downward excitation force, the piston in the upward movement decreased its speed rapidly and began to move in the reverse direction. The abrupt variation in the piston's direction impacted the hydraulic impact force of the head end of the hydraulic cylinder. This increased the pressure of the head end. At this instant, the maximum upward exciting force could reach 12 kN. The above analysis reveals that the hydraulic impact force generated at the instant when the working state of the vibrator was switched could significantly improve the excitation force output of the system while simultaneously producing a bidirectional asymmetric vibration.

It is evident from Figure 11(c) that the flow trends of the two cavities of the hydraulic cylinder were symmetrical while reaching a steady-state vibration. However, the head-end flow amplitude was evidently higher than that of the rod end. This is in line with the laws of single-rod hydraulic cylinder work. Furthermore, in the direction of the hydraulic vibrator switch, the flow surged in the shortest time to attain the corresponding cycle amplitude. Moreover, an increase in the

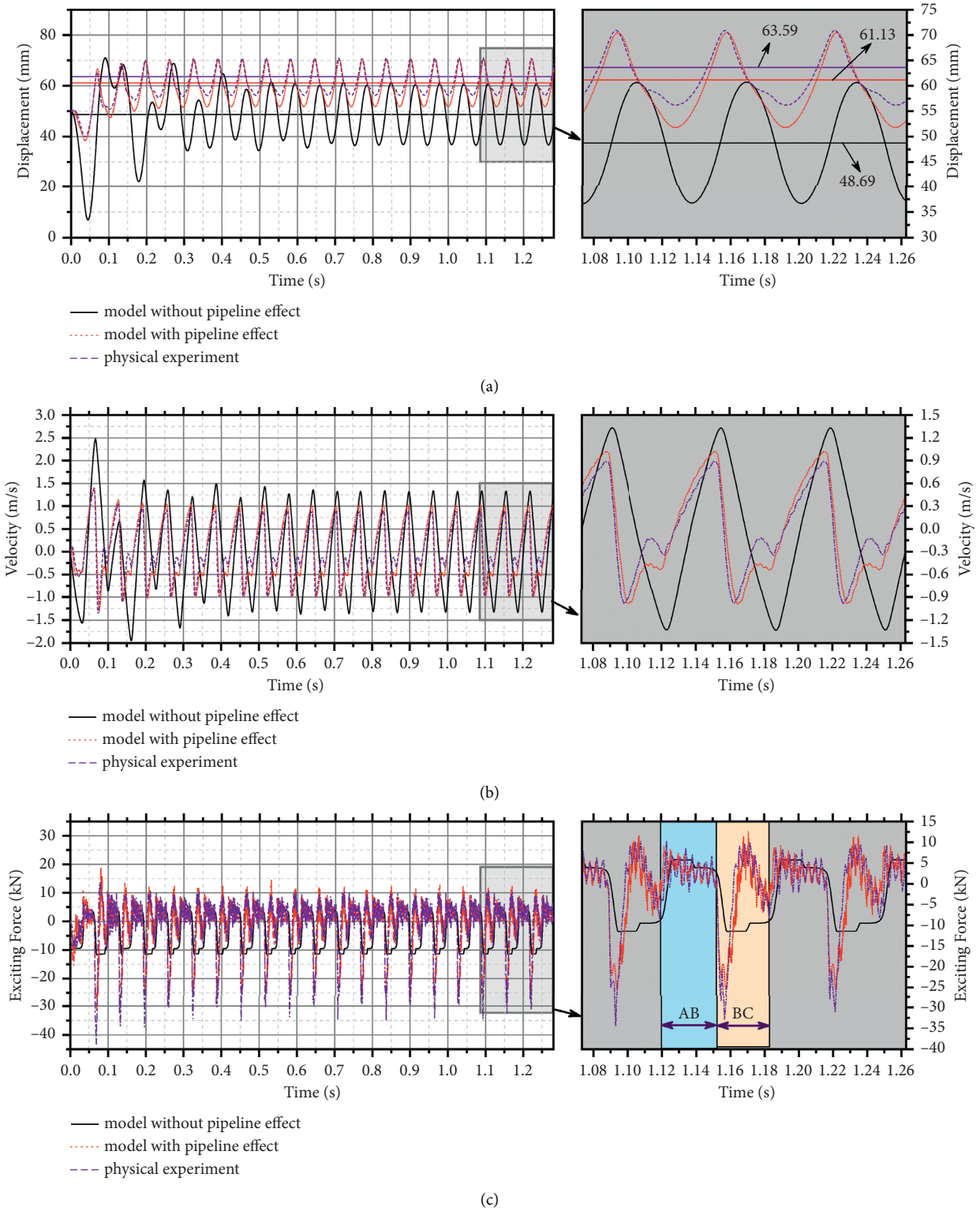

Figure 10: Comparison of the solutions obtained using the two computational models with the experimental measurements. (a) Displacement. (b) Velocity. (c) Excitation force.

Table 3: Characteristic physical quantities of the vibration waveforms.

Physical quantity	Experiment	Model without pipeline effect		Model with pipeline effect	
		Value	Error ratio (%)	Value	Error ratio (%)
Double amplitude	14.77 mm	24.07 mm	62.9	18.67 mm	26.4
Vibrating center	63.59 mm	48.69 mm	23.4	61.13 mm	3.8
Wave peak	70.97 mm	60.72 mm	14.4	70.46 mm	0.7
Wave trough	56.20 mm	36.65 mm	34.8	51.79 mm	7.8
Maximum upward velocity	0.89 m/s	1.33 m/s	49.4	1.02 m/s	14.6
Maximum downward velocity	0.99 m/s	1.33 m/s	34.3	1.01 m/s	3.0

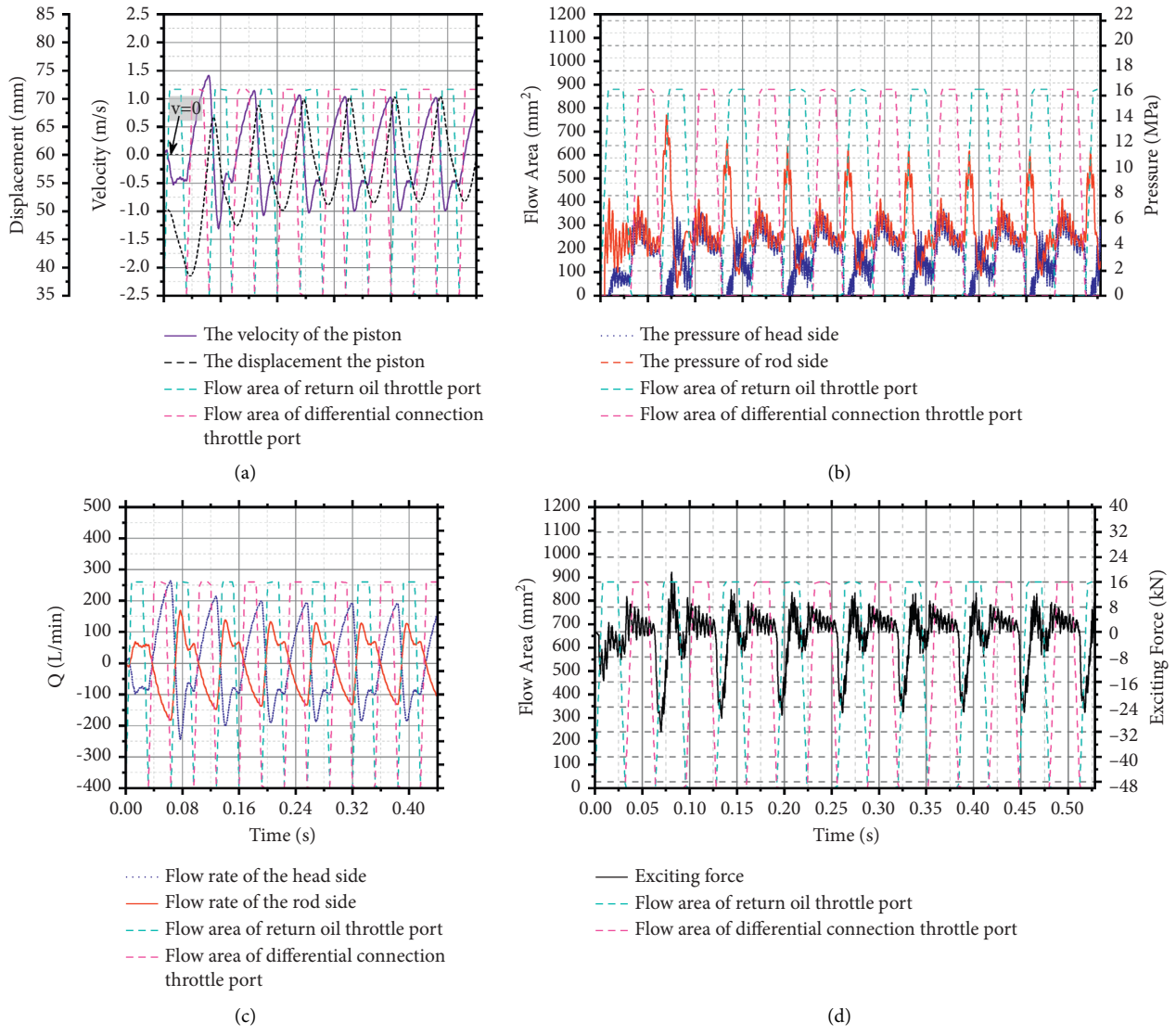

Figure 11: Variation of output parameters of the excitation system with the orifice area of the vibrator. (a) Displacement and velocity. (b) Pressures of two cavities of the cylinder. (c) Excitation force. (d) Flow rate of the two cavities of the cylinder.

flow rate implied that the amplitude of the vibration system had increased.

5.3. Influences of Various Parameters on the System. After verifying the effectiveness of the system model with the pipeline effect, it was used to study the influence of different operating parameters on the output characteristics of the excitation system. Specifically, the effects of the oil supply pressure, spindle speed, load, vibration spring stiffness, and precompression length on the output waveform and excitation force were analyzed. The above parameters in the computational model were initially set as follows: oil supply pressure = 3 MPa, set value of the frequency converter = 5,

excitation load mass = 100 kg, vibration spring stiffness = 180,000 N/m, and precompression length = 2 cm.

5.3.1. Influence of Oil Supply Pressure. The output characteristics of the system under different liquid supply pressures were compared by setting the opening pressure of the relief valve to three levels (namely, 3, 5, and 8 MPa) and maintaining the other parameters at their initially set values.

The outputs of the excitation system vibration under different pressures were periodic, and the amplitudes were positively correlated with the fluid pressure (see Figure 12(a)). When the system pressure was set to 3, 5, and 8 MPa, the double amplitudes of the excitation system were 32.90, 48.48, and 68.80 mm, respectively. However, it was limited by the hydraulic cylinder stroke. When the system pressure reached 5 MPa, the movement of the piston was constrained by the cylinder body. This resulted in the transformation of the vibrating center from an upward to a downward bias. Moreover, the rotational position of the rotary valve corresponding to the highest and lowest points of the piston shifted forward with an increase in the setting pressure. This indicates that the higher the oil supply pressure is, the more advanced the occurrence time of the maximum pressure shock wave is.

As shown in Figure 12(b), the output forces of the excitation system in all the cases exhibited a certain periodicity under different system pressures. Moreover, the variation trends within the same period were broadly consistent. The output force of the excitation system increased gradually with an increase in the oil pressure. Meanwhile, the hydraulic impact force caused by the state switch of the hydraulic vibrator increased significantly with an increase in the system pressure, and its occurrence time was advanced.

5.3.2. Influence of Spindle Speed. Here, the initial settings of the system parameters were maintained, and the set values of the motor frequency converter were altered to 5, 8, 11, and 14. The corresponding spindle speeds were 144, 230.4, 316.8, and 403.2 r/min, respectively. Based on the above analysis, the excitation frequency of the system essentially coincided with the rotating circular frequency of the spindle. Hence, the excitation frequency of the system model was $f = 1/T = (1.44 \times n)$ Hz.

Figure 13(a) shows that the vibration frequency of the excitation system matched well with the circular frequency of the spindle. Therefore, the excitation system could realize real-time frequency conversion in the excitation process, with a variation in the motor speed. The output amplitude of the system decreased gradually as the excitation frequency increased. At frequencies of 7.2, 11.52, 15.84, and 2016 Hz, the output dual amplitudes of the system were 32.90, 18.76, 12.41, and 8.60, respectively. In addition, the vibration center of the hydraulic cylinder decreased gradually as the excitation frequency increased, with the decreasing trend becoming slower gradually.

A comparison of the output force of the excitation system at different frequencies shown in Figure 13(b) reveals that it maintained good periodicity at different frequencies. However, the influence of the pipeline effect became increasingly stronger with an increase in the excitation frequency. This implied that the hydraulic impact force had a higher influence on the exciting force output of the system. In addition, the basic exciting force of the system increased with an increase in the frequency. Therefore, the excitation force also increased with an increase in the spindle speed.

5.3.3. Influence of Load. The vibration actuator of the excitation system adopted a vertical differential oil cylinder, which altered the external load force of the system by varying the load mass. Four load masses were set: 50, 100, 150, and 200 kg. The initial settings of the other system parameters were maintained, and the effect of different loads on the output characteristics of the excitation system was investigated.

The vibration waveform shown in Figure 14(a) reveals that the center position of the output vibration of the system varied significantly under different loads. As the load increased, the vibration center gradually shifted downward. However, this trend gradually slowed down. A comparison of the single-cycle vibration waveforms under different loads revealed that the peak and valley values were delayed as the load increased. This was because the inertia force (which is positively related to the load) affected the movement of the output end of the vertical cylinder. When the load mass was increased from 50 to 200 kg at intervals of 50 kg, the double amplitudes of the system output vibration were 33.08, 32.90, 31.55, and 29.87 mm, respectively. Thus, it was observed that the output vibration amplitude of the system gradually decreased with an increase in the load.

The excitation force output of the system under different loads is shown in Figure 14(b). The load variations did not affect the periodicity of the exciting force. However, with the increase in the load, the impact of the pressure shock caused by the transient flow of the pressurized pipeline gradually strengthened the system exciting force. This was because the load stiffness of the piston increased with the load. Therefore, under an identical rule for throttle-port opening and closing, the phenomenon of water hammer would intensify. This would result in a higher hydraulic impact.

5.3.4. Influence of Spring Stiffness. The vibration spring provided a certain elastic load for the excitation system. It depended on the stiffness of the spring. Therefore, as the next step in the analysis, the vibration output characteristics of an excitation system with different spring stiffness were compared. The other system parameters of the simulation model were consistent with the initial settings. The spring stiffness was assigned six values in the range of 100,000–300,000 N/m in steps of 40,000 N/m.

The vibration waveform outputs of the excitation system under the different spring stiffness values were similar to a sine wave with consistent periodicity (see Figure 15(a)). However, a phase difference existed among the vibration waveforms under different stiffness values. That is, as the stiffness increased, the leading phase of the vibration waveform increased gradually, and the distortion rate of the

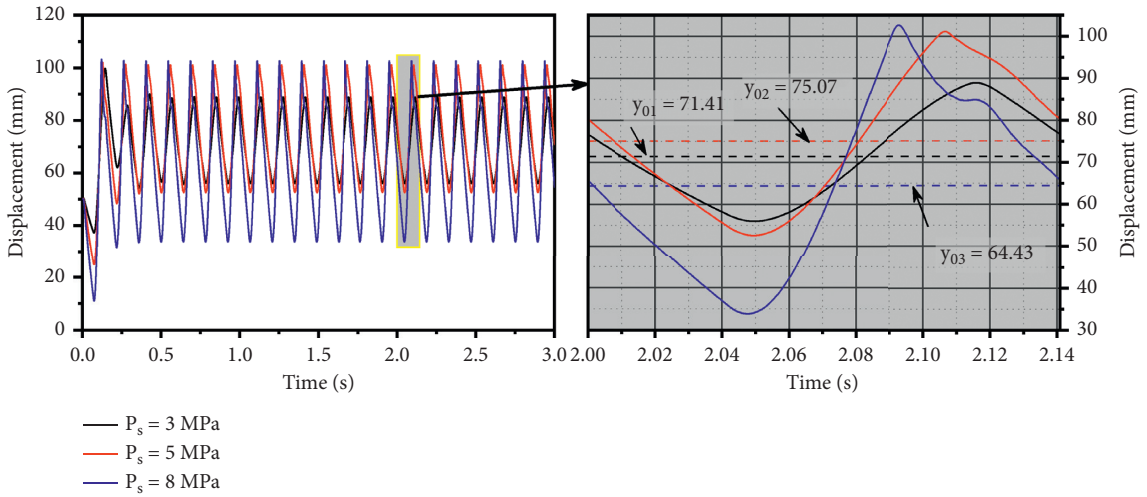

(a)

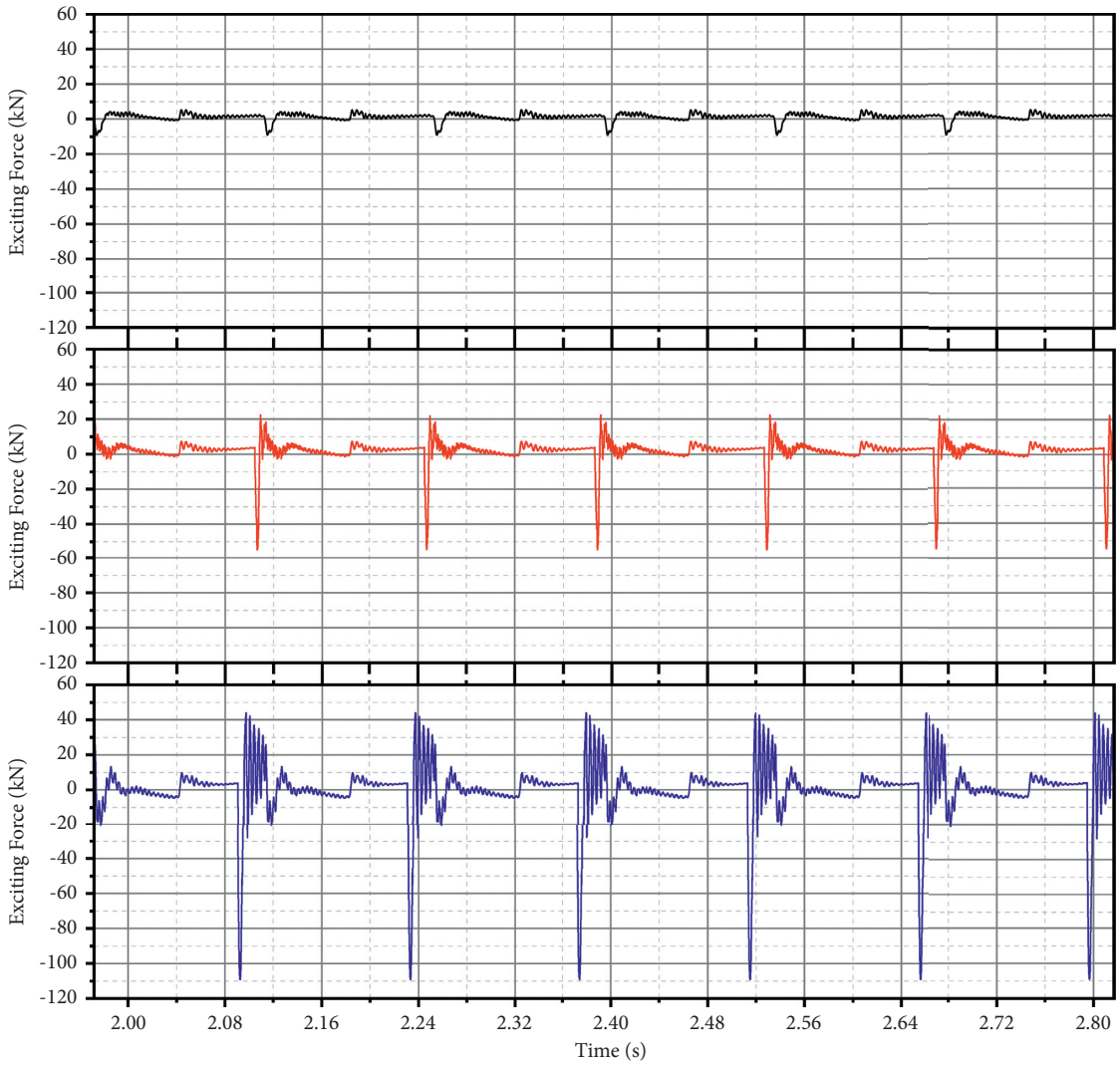

(b)

Figure 12: Trends of (a) output displacements and (b) excitation force under different oil supply pressures.

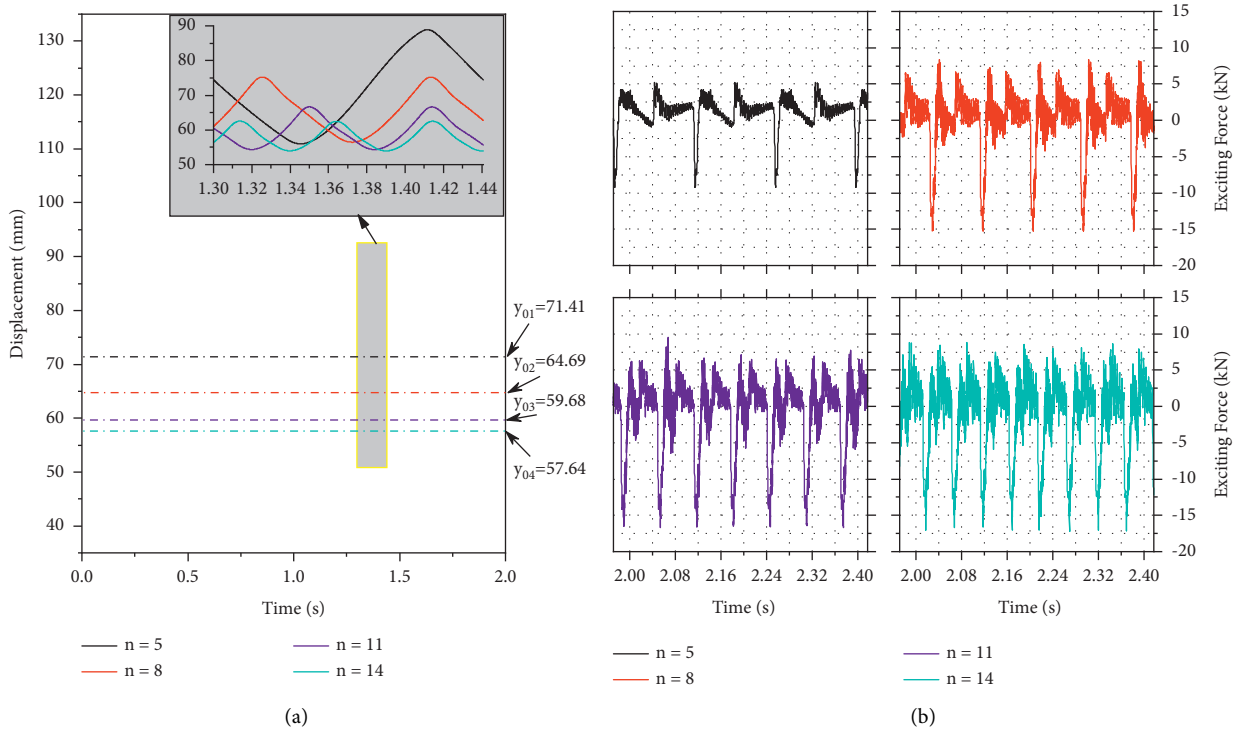

Figure 13: Trends of (a) output displacements and (b) excitation force under different spindle speeds.

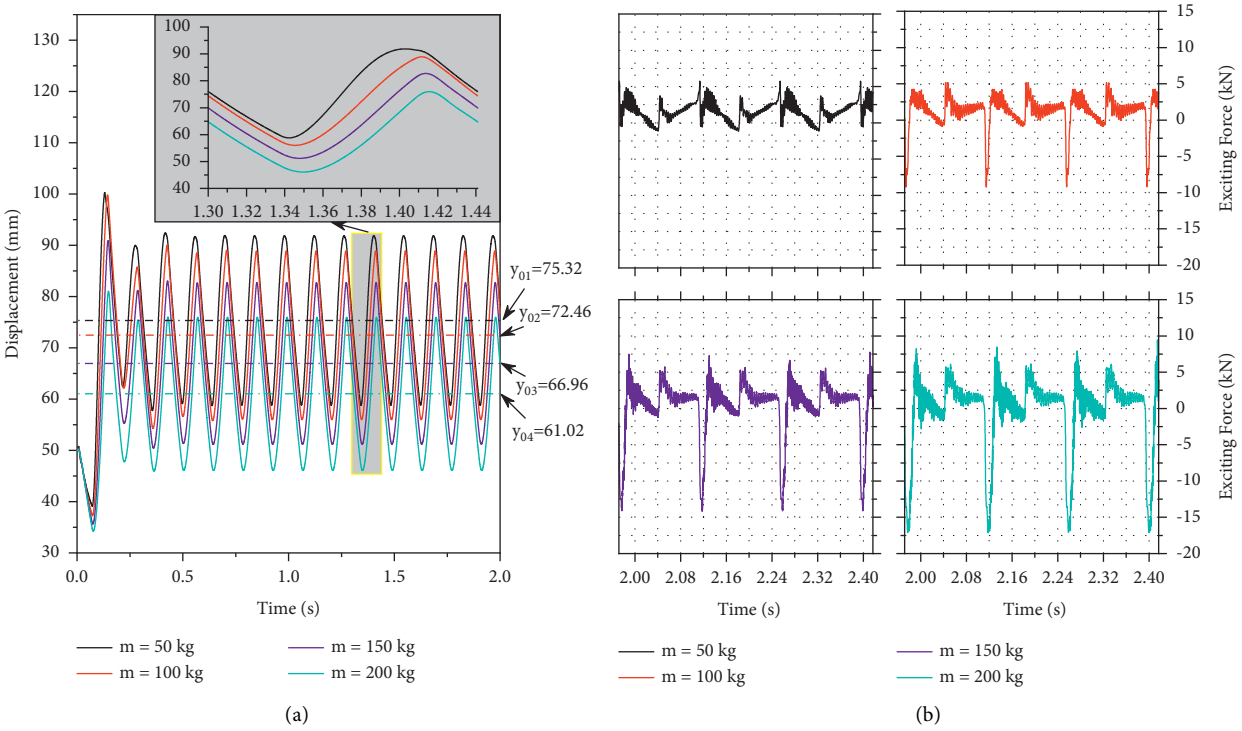

Figure 14: Trends of (a) output displacements and (b) excitation force under different loads.

vibration waveform relative to the sine wave reduced. The output double amplitudes of the excitation system under the aforementioned six spring stiffness values were 32.61, 32.80, 32.90, 32.77, 32.47, and 32.10 mm, respectively. Thus, it can be observed that the amplitude increased at first and then decreased when the spring stiffness increased. The variation

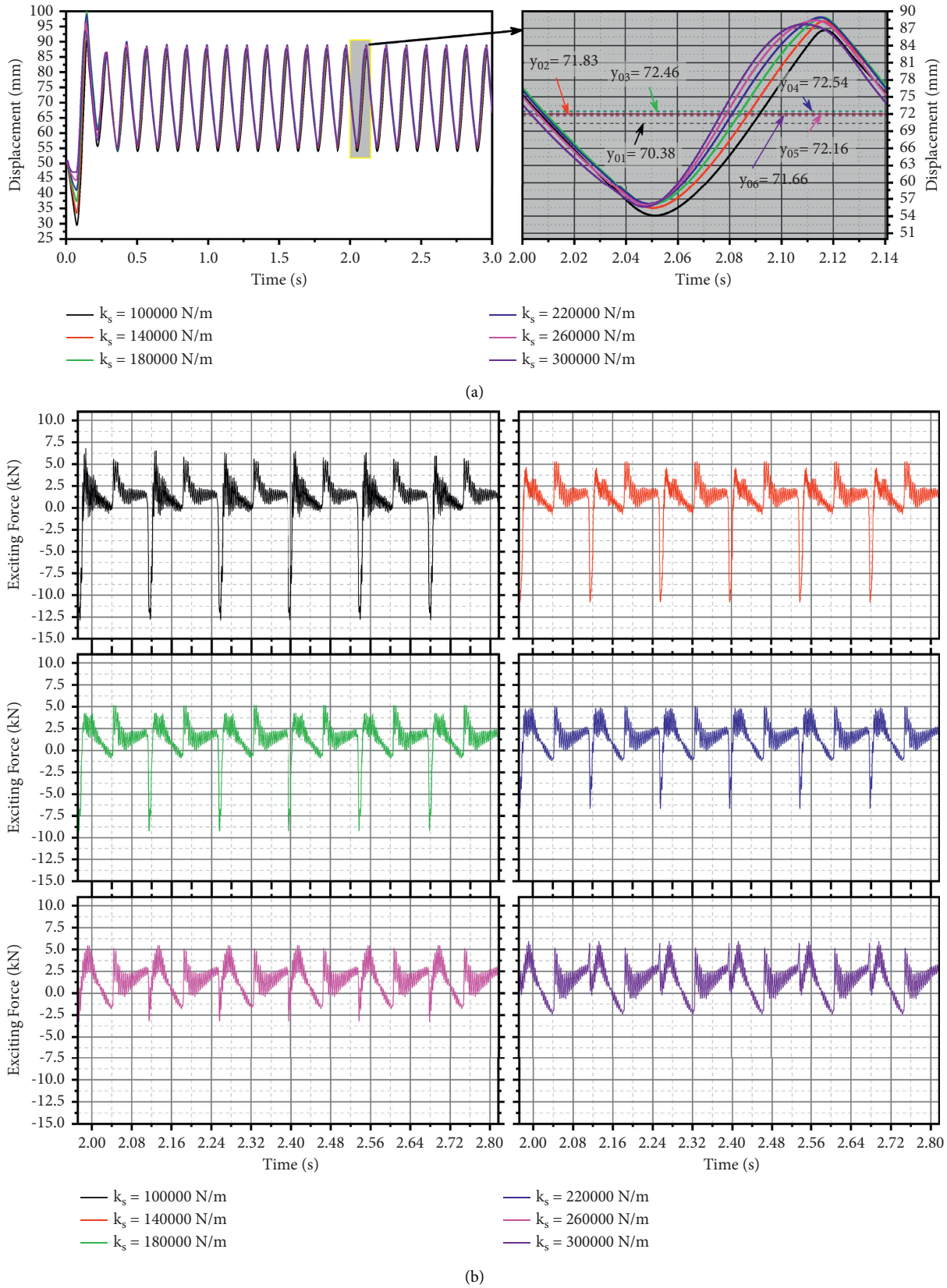

Figure 15: Trends of (a) output displacements and (b) excitation force under different values of spring stiffness.

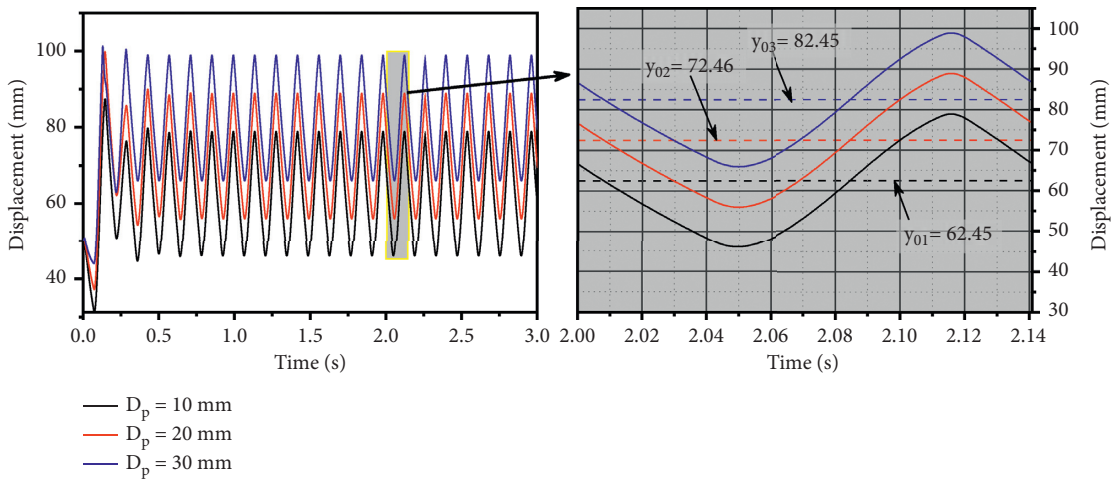

(a)

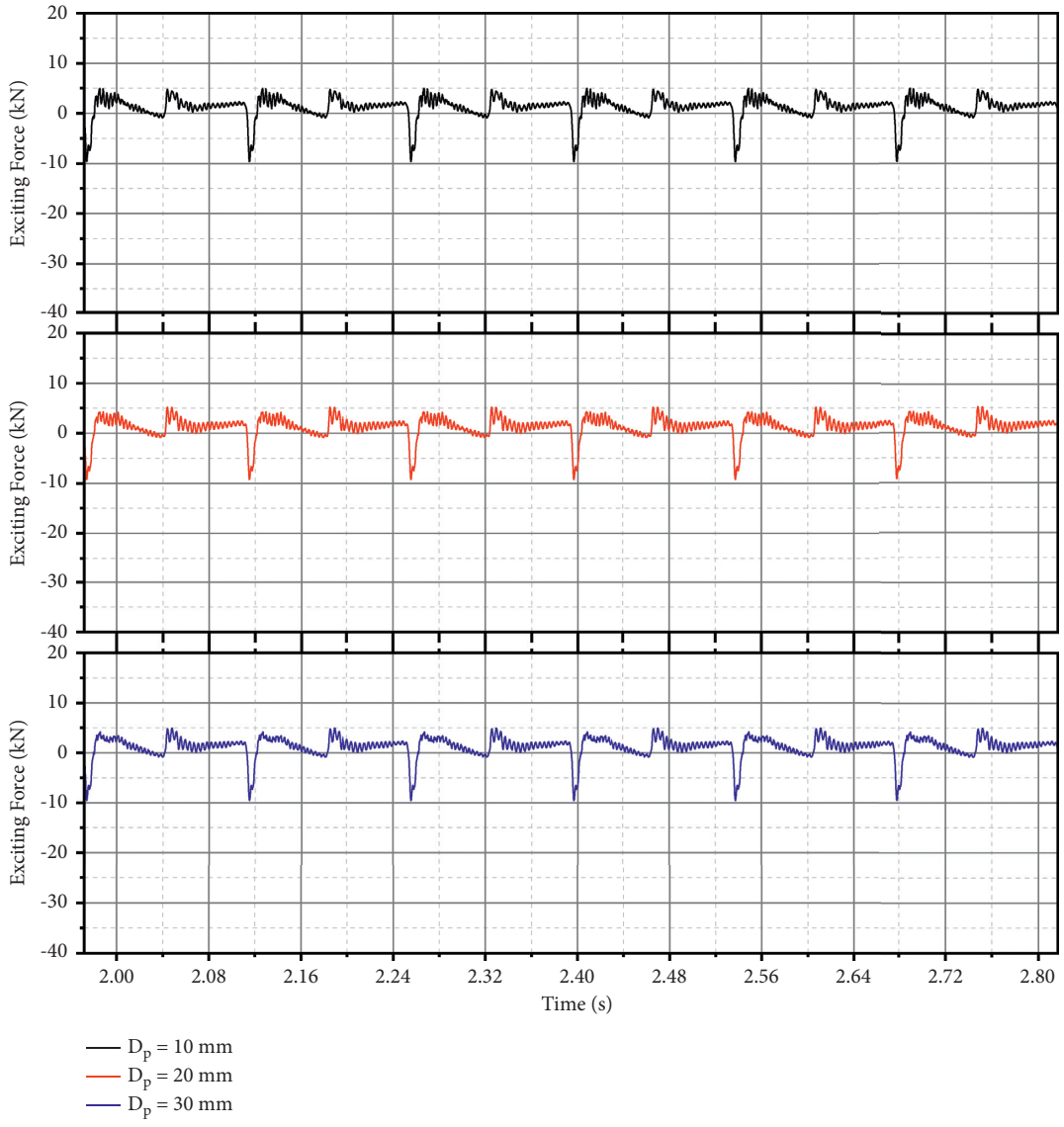

(b)

Figure 16: Trends of (a) output displacements and (b) excitation force under different precompressed spring lengths.

trend of the deviation in the equilibrium position of system vibration was consistent with the variation in amplitude. An inflection point existed between 220,000 and 260,000 N/m. Therefore, it can be concluded that the vibration system could produce the maximum amplitude with the other parameters remaining unaltered, and that the equilibrium position attained the lowest point. That is, the equilibrium position of the system could be optimized by varying the spring stiffness, but with a boundary limitation.

The spring provided an elastic load for the excitation system and functioned as a capacitive element of the mechanical force. Therefore, different values of spring stiffness affected the excitation force output of the system. Figure 15(b) shows that the fundamental excitation force output of the system increased with an increase in the stiffness. However, the influence of the hydraulic impact on the exciting force decreased gradually. This indicates that the higher the spring stiffness is, the larger the hydraulic impact force in the excitation system that can be absorbed. Moreover, the hydrostatic exciting force of the system can be increased simultaneously.

5.3.5. Influence of Precompressed Length of Spring. A variation in the precompressed length of the spring could alter the elastic load in the excitation system, i.e., the initial conditions of the system. Two other comparison groups were formed by setting the precompressed length in the system to 10 and 30 mm while maintaining the initial setting of the system. The displacement and excitation force output by the three vibration systems were obtained and are shown in Figure 16.

As shown in Figure 16(a), the vibration waveform of the system did not change. For example, the characteristic physical quantities, such as amplitude and phase, were almost constant. However, the offset of the vibration center with a variation in the precompressed length and the excitation force output of the excitation system were completely consistent under different precompressed lengths. Figure 16(b) shows that the variation in the precompressed length did not substantially impact the pressure variations in the system. Therefore, the excitation system could alter the position of different excitation forces in space by adjusting the precompressed length of the spring without affecting the vibration output of the system.

6. Conclusions

In this study, a hydraulic vibration-excitation system comprising a vertical asymmetric hydraulic cylinder and hydraulic shock rotary vibrator was proposed. Two types of models of the system were established: one considering the pipeline effect and the other without considering it. The validity of these two system models was verified experimentally. The switching of the working state of the vibrator and influence of system parameters, such as oil supply pressure, spindle speed, load, stiffness of the spring, and precompressed spring length, on the system output were investigated. The conclusions are as follows:

(1) The flow area of the rotary vibrator used in the vibration-excitation system proposed in this study and the flow gain of its throttle port were improved significantly through a structural design of the multilayer valve sleeve. This enabled the system to produce a controllable hydraulic shock force in the excitation process. This part of the hydraulic shock force and the static pressure of the system together constituted the excitation force output of the system.

(2) The pipeline effect had a crucial influence on the output characteristics of the vibration-excitation system. Therefore, it needs to be considered in the modeling of hydraulic systems with high-frequency variations in the velocity and flow direction of the working fluid to prevent large errors in the system output.

(3) When the working state of the rotary vibrator was switched, the pressure in both the working chambers of the differential cylinder increased significantly. In particular, when the stiffness of the spring was appropriate and the vibrator was switched from the differential working state to oil-return working state, the flow rate in both the chambers increased abruptly, and the pressure in the rod chamber of the hydraulic cylinder increased instantaneously to more than two times the system pressure. This significantly improved the excitation force output of the system. In addition, it caused the system to produce a bidirectional asymmetric vibration, which is favorable for engineering applications requiring coupling effect of vibration and impact.

(4) The excitation frequency of the system relied completely on the rotational speed of the spindle of the vibrator. Therefore, a step-less frequency conversion of the system could be realized by varying the rotational speed of the motor controlled by the vibrator. The amplitude of the system output vibration decreased gradually with an increase in the frequency and load. However, it could be increased by increasing the system oil supply pressure. The stiffness coefficient of the vibration spring and its preload had relatively insignificant influence on the amplitude. However, an optimal spring stiffness could ensure that the system produced maximum amplitude under identical parameters. Furthermore, the equivalent offset of the vibration center could be realized by altering the precompressed spring length.

(5) With increases in the oil supply pressure, excitation frequency, and load, the hydraulic shock in the system would be strengthened and the static pressure during the vibration would increase. Therefore, the excitation force output of the system would also increase. However, a vibration spring with a higher stiffness can significantly restrain this hydraulic shock and decrease the hydraulic shock force in the system significantly. Nevertheless, the fundamental excitation force output of the system would increase.

Our future work will focus on the coupling relationship between the variable parameters of the vibration-excitation system and its output, identify optimal working parameters, and explore successful engineering applications of the proposed vibration-excitation system.

Nomenclature

R: Radius of hollow spindle
r: Radius of semicircle at both ends of throttle
α: Central angle corresponding to two groove intervals
β: Central angle corresponding to bottom arc length of each trapezoidal groove
N: Number of grooves
θ: Rotation angle of hollow spindle
p_s: Oil supply pressure
p_t: Oil-return pressure
p_1: Pressure of rear end of cylinder
p_2: Pressure of rod end of cylinder
Q_0: Oil supply flow rate
Q_1: Outflow rate of rear end of cylinder
Q_2: Inflow rate of rod end of cylinder
Q_{L1}: Flow rate of throttle of vibrator in its differential connection state
Q_{L2}: Flow rate of throttle of vibrator in its oil-return connection state
C_e: External leakage coefficient of cylinder
C_i: Internal leakage coefficient of cylinder
l_{s0}: Stroke of piston rod
l_0: Original length of vibration spring
D_p: Precompression length of spring
y_p: Displacement of piston rod
C_d: Flow coefficient of throttle
Q_L: Load flow of system
ρ: Density of oil
k: Bulk modulus of oil
B_p: Viscous friction coefficient
k_s: Stiffness coefficient of vibration spring
H: Water head
τ_0: Frictional resistance of pipeline
f: Darcy frictional resistance coefficient
N_s: Spindle speed
N_r: Rated speed of motor.

Data Availability

Relevant research data can be obtained upon request from the corresponding author.

Conflicts of Interest

The authors declare that there are no potential conflicts of interest with respect to the research, authorship, and/or publication of this article.

Authors' Contributions

All the authors contributed to the conceptualization and design of the study. Material preparation, data collection, and analysis were performed by Qichao Ren, Ziming Kou, Juan Wu, and Tengyu Li. The first draft of the manuscript was written by Qichao Ren, and all the authors provided inputs for the initial versions of the manuscript. All the authors have read and approved the final manuscript.

Acknowledgments

This study was supported by the National Natural Science Foundation of China (grant no. U1910212), Shanxi Key Research and Development Project of China (grant no. 201903D121078), and Shanxi Fundamental Research Project of China (grant no. 201901D211009).

Supplementary Materials

The appendix explains the nomenclature of symbols contained in all the formulas in this paper. (*Supplementary Materials*)

References

[1] Y. Wu, S. Li, S. Liu, H.-S. Dou, and Z. Qian, *Vibration Induced by Hydraulic Excitation*, Springer Science and Business Media B.V., Dordrecht, Netherlands, pp. 147–233, 2013.
[2] C. Sihler, "A novel torsional exciter for modal vibration testing of large rotating machinery," *Mechanical Systems and Signal Processing*, vol. 20, no. 7, pp. 1725–1740, 2006.
[3] Q. Song, Z. Yang, and W. Wang, "Robust control of exciting force for vibration control system with multi-exciters," *Science China Technological Sciences*, vol. 56, no. 10, pp. 2516–2524, 2013.
[4] Y. Guo, D. Liu, S. Yang, X. Li, and J. Chen, "Hydraulic–mechanical coupling modeling by bond graph for impact system of a high frequency rock drill drifter with sleeve distributor," *Automation in Construction*, vol. 63, pp. 88–99, 2016.
[5] Y. Hu, J. Zhao, J. Zhao et al., "Coiled tubing friction reduction of plug milling in long horizontal well with vibratory tool," *Journal of Petroleum Science and Engineering*, vol. 177, pp. 452–465, 2019.
[6] S. Pagano, M. Russo, S. Strano, and M. Terzo, "A mixed approach for the control of a testing equipment employed for earthquake isolation systems," *Proceedings of the Institution of Mechanical Engineers - Part C: Journal of Mechanical Engineering Science*, vol. 228, no. 2, pp. 246–261, 2013.
[7] H. Shahverdi, C. Mares, and J. E. Mottershead, "Model structure correction and updating of aeroengine casings using fictitious mass modifications," *Proceedings of the Institution of Mechanical Engineers - Part C: Journal of Mechanical Engineering Science*, vol. 219, no. 1, pp. 19–30, 2016.
[8] Y. Liu, T. Wang, G. Gong, and R. Gao, "Present status and prospect of high-frequency electro-hydraulic vibration control technology," *Chinese Journal of Mechanical Engineering*, vol. 32, pp. 1–16, 2019.
[9] W. Li, G. Gong, Y. Zhang, J. Liu, Y. Chen, and F. Wang, "Development and parameters analysis of hydraulic controlled rotary valve excitation system," *Energies*, vol. 13, pp. 1–23, 2020.
[10] Y. Liu, S.-K. Cheng, and G.-F. Gong, "Structure characteristics of valve port in the rotation-spool-type electro-hydraulic vibrator," *Journal of Vibration and Control*, vol. 23, no. 13, pp. 2179–2189, 2015.

[11] L. Nascutiu, "Voice coil actuator for hydraulic servo valves with high transient performances," in *Proceedings of the IEEE International Conference on Automation. IEEE*, pp. 185–190, Cluj-Napoca, Romania, May 2006.
[12] T. A. Joseph, *Rotary Valve*, US, 2004.
[13] J. J. Sallas, *Low Inertia Servo Valve*, US, 1995.
[14] C. Andrew and M. Martin, *Rotary Servo Valve*, UK, 2020.
[15] H. Wang, G. Gong, H. Zhou, and W. Wang, "Steady flow torques in a servo motor operated rotary directional control valve," *Energy Conversion and Management*, vol. 112, pp. 1–10, 2016.
[16] H. Wang, G. Gong, H. Zhou, W. Wang, and Y. Liu, "A rotary valve controlled electro-hydraulic vibration exciter," *Proceedings of the Institution of Mechanical Engineers - Part C: Journal of Mechanical Engineering Science*, vol. 230, no. 19, pp. 3397–3407, 2016.
[17] H. Wang, C. Wang, L. Quan, G. Gong, and W. Li, "Analytical solution to orifice design in a rotary valve controlled electro-hydraulic vibration exciter for high-frequency sinusoidal vibration waveform," *Proceedings of the Institution of Mechanical Engineers - Part E: Journal of Process Mechanical Engineering*, vol. 233, no. 5, pp. 1098–1108, 2019.
[18] J. Ruan, "Electrohydraulic vibration exciter controlled by 2D valve," *Journal of Mechanical Engineering*, vol. 45, no. 11, pp. 125–131, 2009.
[19] J. Ruan and R. T. Burton, "An electrohydraulic vibration exciter using a two-dimensional valve," *Proceedings of the Institution of Mechanical Engineers - Part I: Journal of Systems & Control Engineering*, vol. 223, no. 2, pp. 135–147, 2008.
[20] Y. Ren and J. Ruan, "Theoretical and experimental investigations of vibration waveforms excited by an electro-hydraulic type exciter for fatigue with a two-dimensional rotary valve," *Mechatronics*, vol. 33, pp. 161–172, 2016.
[21] Y. Ren, J. Ruan, and J. Wa, "Bias control strategy for electro-hydraulic vibration exciter with two-dimensional valve," *Hsi-An Chiao Tung Ta Hsueh/Journal of Xi'an Jiaotong University*, vol. 44, pp. 82–86, 2010.
[22] Y. Ren, H. Tang, and J. Xiang, "Experimental and numerical investigations of hydraulic resonance characteristics of a high-frequency excitation system," *Mechanical Systems and Signal Processing*, vol. 131, pp. 617–632, 2019.
[23] J. Yu, J. Zhuang, and D. Yu, "Modeling and analysis of a rotary direct drive servovalve," *Chinese Journal of Mechanical Engineering*, vol. 27, no. 5, pp. 1064–1074, 2014.
[24] Y. Yang, E. Guglielmino, J. S. Dai, T. Boaventura, and D. G. Caldwell, "Modeling of a novel 3-way rotary type electrohydraulic valve," in *Proceedings of the 2010 IEEE International Conference on Information and Automation, ICIA 2010*, pp. 1463–1468, IEEE Computer Society, Harbin, China, June, 2010.
[25] I. Okhotnikov, P. S. Noroozi, S. Noroozi, P. Sewell, and P. Godfrey, "Evaluation of steady flow torques and pressure losses in a rotary flow control valve by means of computational fluid dynamics," *International Journal of Heat and Fluid Flow*, vol. 64, pp. 89–102, 2017.
[26] Y. Liu and X. Ji, "Simulation of cavitation in rotary valve of hydraulic power steering gear," *Science in China - Series E: Technological Sciences*, vol. 52, no. 11, pp. 3142–3148, 2009.
[27] E. Lisowski and J. Rajda, "CFD analysis of pressure loss during flow by hydraulic directional control valve constructed from logic valves," *Energy Conversion and Management*, vol. 65, pp. 285–291, 2013.
[28] W. Zhang, H. Shi, G. Li, and X. Song, "Fluid hammer analysis with unsteady flow friction model in coiled tubing drilling," *Journal of Petroleum Science and Engineering*, vol. 167, pp. 168–179, 2018.
[29] E. B. Wylie and V. L. Streeter, *Fluid Transients in Systems*, Prentice-Hall, Hoboken, NJ, USA, 1993.
[30] H. X. Zhang, Z. M. Kou, J. Wu, and C. Y. Lu, "Numerical simulation and analysis of hydraulic excitation system based on water hammer by the method of characteristics," *Advanced Materials Research*, vol. 295–297, pp. 2210–2215, 2011.
[31] C. Lu, Z. Kou, J. Wu, and H. Zhang, "Dynamic characteristics of pipes conveying fluid excited by hydraulic fluctuation," *Huazhong Keji Daxue Xuebao (Ziran Kexue Ban)/Journal of Huazhong University of Science and Technology (Natural Science Edition)*, vol. 41, pp. 17–22, 2013.